2D Transition Metal Carbides (MXenes) for Carbon Capture

Persson, Ingemar; Halim, Joseph; Lind, Hans; Hansen, Thomas W.; Wagner, Jakob B.; Näslund, Lars-Åke; Darakchieva, Vanya; Palisaitis, Justinas; Rosen, Johanna; Persson, Per O.Å.

Published in:
Advanced Materials

Link to article, DOI:
10.1002/adma.201805472

Publication date:
2019

Document Version
Peer reviewed version

2D transition metal carbides (MXenes) for carbon capture

Ingemar Persson,*[1] Joseph Halim,[1] Hans Lind, [1] Thomas W. Hansen[2], Jakob B. Wagner,[2] Lars-Åke Näslund,[1] Vanya Darakchieva,[3] Justinas Palisaitis,[1] Johanna Rosen[1] and Per O. Å. Persson[1]

[1] Thin Film Physics Division, Department of Physics, Chemistry and Biology (IFM), Linköping University, SE-581 83 Linköping, Sweden

[2] Center for Electron Nanoscopy, DTU Danchip/CEN, DK-2800, Kgs. Lyngby, Denmark

[3] Terahertz Materials Analysis Center (THeMAC), Department of Physics Chemistry and Biology (IFM), Linköping University, SE-581 83 Linköping, Sweden

Keywords

MXene, surface terminations, carbon capture, environmental TEM

Global warming caused by burning of fossil fuels is indisputably one of mankind's greatest challenges in the twenty-first century. To reduce the ever-increasing CO_2 emissions released into the atmosphere, dry solid adsorbents with large surface to volume ratio such as carbonaceous materials, zeolites, and metal organic frameworks have emerged as promising material candidates for capturing CO_2. However, challenges remain because of limited CO_2/N_2 selectivity and long-term stability. The effective adsorption of CO_2 gas (~12 mol kg^{-1}) on individual sheets of two-dimensional (2D) transition metal carbides (referred to as MXenes) is reported here. It is shown that exposure to N_2 gas results in no adsorption, consistent with first-principle calculations. The adsorption efficiency combined with the CO_2/N_2 selectivity, together with a chemical and thermal stability, identifies the archetype Ti_3C_2 MXene as a new material for carbon capture (CC) applications.

In the search for new solid adsorbents that can capture carbon dioxide by physical and chemical adsorption, focus is turned to materials with high surface area including carbonaceous materials, [1] zeolites, [2] metal organic frameworks, [3] and 2D materials such as functionalized graphene oxide. [4] Despite several advantages (moles adsorbed per mass unit, low production cost), they are challenged by poor selectivity for CO_2 over N_2 and robustness in terms of lifetime and multicycle durability. [5] MXenes are a recent addition to the family of 2D materials and have emerged with superior properties and performance in terms of stability, [6] electrochemical charge storage, [7,8] electromagnetic interference shielding, [9] filtering, [10] and a range of additional applications. [8]

They constitute a large and growing family of 2D materials, [11,12] that are obtained from the laminated $M_{n+1}AX_n$ (MAX) phases (M is a transition metal, A is a group A element -mostly group 13 and 14 - and X is C and/or N) [13] by chemical etching of the atomically thin A element layers that separate sheets of $M_{n+1}X_n$. As the A-element is removed, the MXene surfaces are immediately functionalized by surface terminating species, T_x. [6,14] Hence the proper MXene formula is $M_{n+1}X_nT_x$. Accordingly, the MXene properties can be tuned through structure, intrinsic composition, and surface terminations. The structure is inherited from the parent MAX phase (hexagonal, space group $P6_3/mmc$) but compositional tuning display an extraordinary toolbox for property tuning through MXenes based on single M and X elements, as well as alloys on both M and X. [12,15] In addition, there are reports on MXenes forming out-of-plane [16] and in-plane [17] double-M elemental ordering, as well as vacancy-ordered structures. [18,19] Manipulation of the surface terminations constitute the final and most powerful variable for property tuning. [20] Despite several theoretical investigations, [21,22,23] non-inherent terminations have remained experimentally unexplored. Currently, the MXene preparation dictates that T_x is inherent to the etchant and predominantly a combination of O and F, where also OH has been considered as a minor [24] or even negligible contribution. [25]

In the area of CC, MXenes are predicted to be highly efficient for capturing CO_2, enabling capture of 2-8 mol CO_2 kg^{-1}. [21,22] However, the MXene surfaces were assumed to be termination free, an experimentally unrealistic starting point, given the current wet-chemical preparation routes for MXenes. To unlock the MXene potential for non-inherent terminations or adsorption of other molecules, such as CO_2, we have subjected the archetype $Ti_3C_2T_x$ MXene to a novel approach. Using *in situ* environmental transmission electron microscopy (ETEM), single $Ti_3C_2T_x$ sheets were subjected to an initial high temperature treatment to desorb F, [25]

and a subsequent H_2 exposure to remove the persistent O from the surfaces. The thereafter termination-depleted MXene was subsequently exposed to CO_2 gas, resulting in the first MXene to be terminated by a non-inherent molecule. Additionally, termination-depleted MXene surfaces were exposed to N_2 gas after which no N adsorption was observed, consequently identifying Ti_3C_2 as highly efficient also in terms of CO_2/ N_2 selectivity.

Figure 1a-d represent a cross-section schematic that illustrates, from left to right, the processing that was applied to the $Ti_3C_2T_x$ MXene in order to reduce the surface terminating species followed by the adsorption of CO_2. Figure 1a describes an as-prepared single $Ti_3C_2T_x$ flake terminated by a disordered mixture ($x > 2$), predominantly consisting of O and F. [244,25] Figure 1b shows how an initial thermal treatment of the sheet at 650 °C for 12 h inside the ETEM at a pressure of 10^{-6} mbar results in the desorption of F (see supplementary information Fig. S1), in line with previous investigations. [25] In response to the desorbed F, the remaining O rearranges itself to cover the surface at the thermodynamically preferred fcc-site (Fig. 1b). [26] With F depleted and only O remaining, the MXene is locally termination-free ($x < 2$). Following this initial thermal procedure, Fig. 1c schematically illustrates the subsequent introduction of 8 mbar H_2 local gas flow parallel to the sample surface during heating to 700 °C for 0.5 h, leading to O depletion. Finally, as shown in Fig. 1d, 3.5 mbar CO_2 is introduced at 100 °C and adsorbed on the depleted surface. The TEM images presented in Fig. 1e-h demonstrate the single MXene flake structure throughout the *in situ* process, with e) showing the as prepared structure, f) after heating in vacuum, g) after exposure to H_2, and g) after exposure to CO_2 (100 °C was chosen to avoid residual hydrocarbon adsorption on the single sheet). Note that the figures and in particular Fig. 1h, are not astigmatic as determined by fast fourier transform (FFT) (presented in supplementary information, Fig. S2), hence the apparent structure is a result of ordering of the CO_2 molecules on the surface.

During the heating and gas exposure experiments inside the ETEM, the changes in the $Ti_3C_2T_x$ surface chemistry and structure were monitored by electron energy-loss spectroscopy (EELS) and electron diffraction (ED). Residual gas analysis (RGA) was employed to monitor reaction products originating from the interactions of the applied gas and the MXene surface species (shown in the supplementary information, Fig. S3). Following vacuum heating to remove the F terminations, Fig. 2a-c show the EELS spectra acquired from single flakes after 8 mbar H_2 exposure for 1 h intervals at RT, 500, 700, and 750 °C for C-K, Ti-L, and O-K respectively. The shape of the C-K edge in Fig. 2a confirms that the chemical environment of C remains

constant throughout the experiment. A gradual chemical shift up to -1 eV is observed for Ti-L_3 and Ti-L_2 above RT that indicates a decrease of O-terminations (caused by reduced charge transfer from Ti to O). [27] The O-K edge is displayed in Fig. 2c, and a -2 eV energy shift is observed above RT. A plausible cause of the negative shift of O-K is H saturation of the surface. Most importantly, the integrated intensity of the O-K edge, corresponding to remaining surface terminations, is being reduced with increased temperature. EELS quantification of the Ti:O ratio yield 3: 2.1 at RT, 3: 1.4 at 500 °C, 3: 1.2 at 700 °C, and 3: 0.6 at 750 °C. The chemical shifts of Ti-L and O-K in combination with the loss of O, clearly describes a decrease of O-terminations caused by active H on the Ti_3C_2 surface. The apparently depleted surface can also be comprehended from Fig. 1g, which exhibits a clean appearance. Figure 2d presents the corresponding ED patterns that verify the preservation of the MXene structure up to 700 °C. At 750 °C the ED patterns confirm the formation of TiC nanoplatelets [28] with similar lattice spacing compared to Ti_3C_2 (see supplemental information, Fig. S2). During the MXene exposure to H_2, RGA detected the formation of H_2O from 500 °C, which is increasing slightly with temperature (see supplementary information, Fig. S3). The formation of H_2O at elevated temperatures correlates well with O-termination depletion which is expected with H_2 reacting with surface bound O.

The results show that H_2 exposure at elevated temperatures is a facile route for removing O-terminations. Consequently, experiments that probe the fundamental MXene properties are attainable. Because of the low pressure (mbar range) of the applied H_2 gas during the limited time frames, complete removal of O was not achieved in these *in situ* experiments. Further depletion is proposed to be attainable at higher H_2 pressures that are not possible in the ETEM. The high temperature vacuum heating and H_2 processes also demonstrate the robust nature of the employed $Ti_3C_2T_x$.

Figure 2e-g presents EELS spectra for the C-K, Ti-L, and O-K edges, respectively, obtained from single MXene flakes after heat treatment and H_2 exposure at 650 °C followed by exposure of 3.5 mbar CO_2 for 0.5 h at 100 °C. The C-K edge integrated intensity and fine structure radically changes upon CO_2 exposure. In particular, the second broad peak centered at 293 eV exhibits a considerable increase in intensity. The Ti-$L_{3,2}$ edge does not reveal significant fine structure changes (symmetry and bonds remain similar after adsorption), though both the Ti-L_3 and Ti-L_2 (particularly the Ti-L_2) edges experience apparent positive chemical shifts. This is indicative of the formation of a chemical bond between the Ti and adsorbed CO_2, resulting in

charge transfer from the Ti to the CO_2. Figure 2g displays a substantial increase in the O-K edge intensity. EELS quantification of the sheet stoichiometries before and after CO_2 exposure yields a Ti:C:O ratio of $3:2:1.45$ and $3:4.3:5.2$, respectively, which approximately corresponds to one adsorbed CO_2 molecule per M surface atom. This is equivalent to an uptake capacity of 12 mol kg^{-1} or a relative increase by 52.7 wt.%.

Competing materials for carbon capture include Mg-MOF-74 [29] and Zeolite X13 [30] where Mg-MOF-74 is reported to adsorb CO_2 equivalent to a weight increase of 35 wt.% at 1 bar (313 K). [29] Zeolite X13 is the benchmark material because of its low cost and a capacity of 22 wt.% at 1 bar (298K) [30] (Details in Table S1). Furthermore, regeneration of zeolite X13 has been reported to be more cost-effective from a long-term perspective than Mg-MOF-74 despite the capacity difference. On that note, MXenes are chemically and thermally stable (as verified here) and therefore exhibit a high potential for regeneration. Thus, the initial assessment of single Ti_3C_2 sheets yields that MXene is on par with, or even outperforms, current CO_2 adsorbents. [1,2,3,29,30]

The potential for MXenes for carbon capture can be further stressed by employing Ti_2C as an example. Should this MXene adsorb the same amount of CO_2 per surface M element, the weight increase would be an astonishing 80 wt.%. Finally, it is straightforward to alloy most MXenes with a few atomic percent of various metals that can increase the catalytic activity in conversion mechanisms.

Figure 2h presents the corresponding ED patterns acquired before and after CO_2 exposure, respectively, again confirming the preservation of the MXene structure. The final structure after CO_2 exposure as shown in Fig. 1h exhibit a streaked surface and this is proposed to originate from the alignment of CO_2 molecules on the MXene surface. As demonstrated above, CO_2 exposure of the O-depleted MXene immediately leads to complete CO_2 saturation of the surface while the 2D structure is maintained. Complementary to the CO_2 exposure, the H_2 exposed surfaces were additionally subjected to N_2 exposure. During these experiments no adsorbed N_2 was detected, indicating that termination-free Ti_3C_2 is highly selective between CO_2 and N_2. This result is explained by our calculations based on density functional theory (DFT) suggesting an endothermic reaction for N_2 dissociation combined with formation of N-terminated MXene (see supporting information for details). Altogether, owing to the adsorption efficiency, the selectivity and the large surface area per mass unit, Ti_3C_2 MXene is shown to be a highly

efficient material for carbon capture, which constitute an entirely new, and extremely promising, application for MXenes.

In summary, in this manuscript we report two fundamental findings: 1) We have identified a route for termination of (adsorption on) Ti_3C_2 MXene by non-inherent species through a combination of heating and H_2 exposure that depleted the Ti_3C_2 surfaces from terminating species. It is postulated that terminations on other MXenes can also be depleted in the same fashion. 2) We have identified single sheets of Ti_3C_2 MXene as a solid adsorbent for carbon capture applications. Following the surface depletion, a subsequent exposure to CO_2, resulted in the adsorption of ~12 mol kg^{-1} CO_2 on the $Ti_3C_2T_x$, a result that is on par with or even outperforms state of the art CO_2 adsorbents at low pressures. It is proposed that, even higher loadings are attainable following H_2 and CO_2 exposure at higher pressures than presently obtained in the ETEM. We also found that the depleted MXene showed no affinity for N_2 gas, consistent with our calculations, making the sheets highly selective towards CO_2 over N_2. Furthermore, a high stability of the MXene throughout the experiments was demonstrated, in line with previous findings. It is proposed that this may be useful in the subsequent conversion of the captured CO_2 and for recycling of the same material in lines with a circular economy. The here presented results enables MXenes as an exceptional and robust breakthrough material for carbon capture.

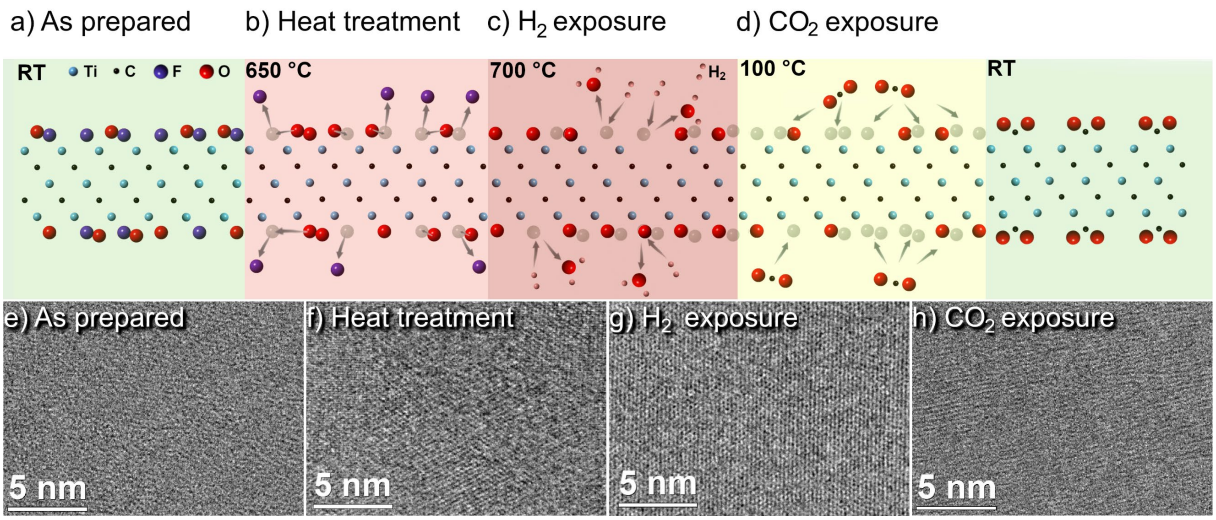

Figure 1. Cross-sectional schematics of a $Ti_3C_2T_x$ flake illustrating the change in surface terminations (evolution of T_x) from left to right, as a result of thermal and environmental processing. a) As prepared, b) heat treatment, c) H_2 exposure, and finally d) CO_2 exposure. The corresponding plan-view TEM images after each step are presented in e-h). The images were acquired at the following conditions; e) as prepared, f) heat treatment for 12 h at 650 °C, g) H_2 exposure for 0.5 h at 8 mbar and 700 °C, and h) CO_2 exposure for 0.5 h at 3.5 mbar and 100 °C.

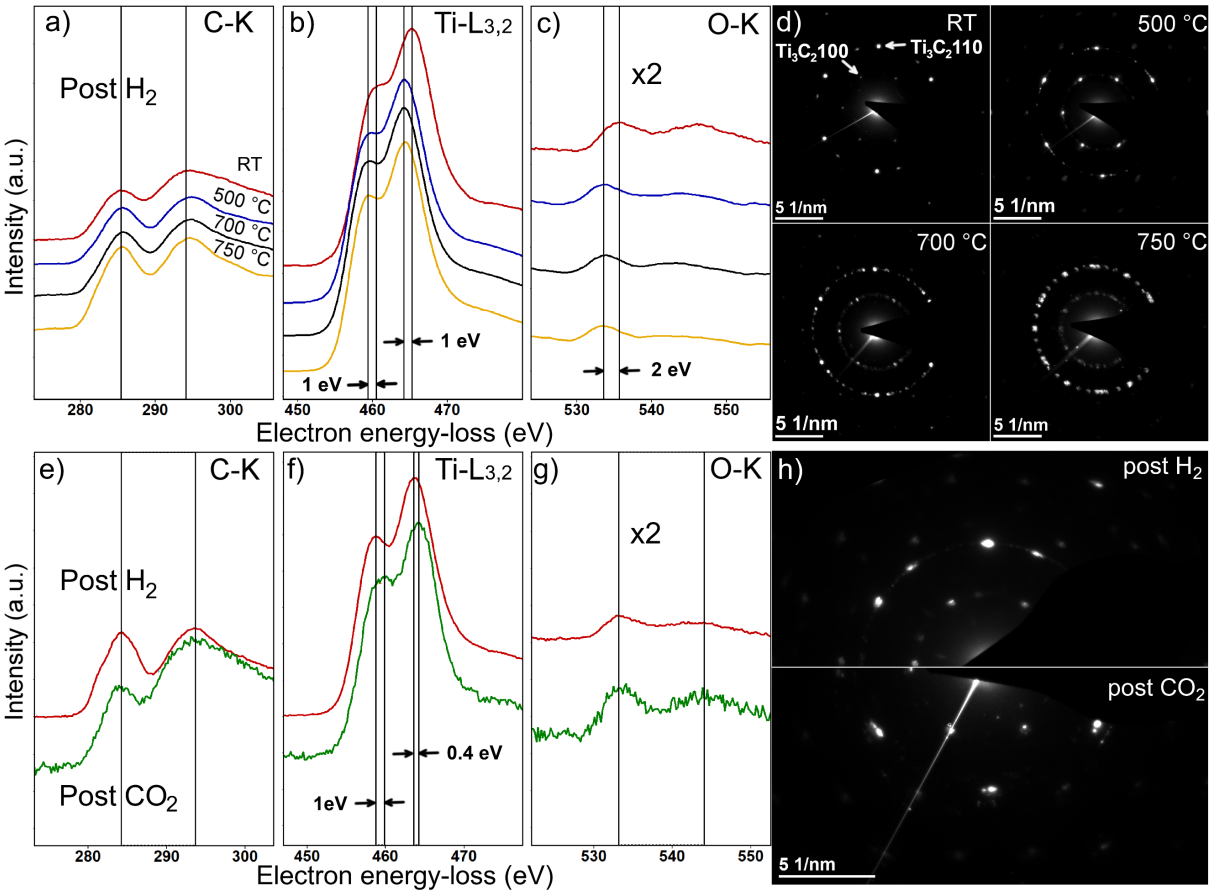

Figure 2. (a-d) EELS spectra and plan-view ED patterns acquired from $Ti_3C_2T_x$ flakes at high vacuum conditions after exposure to 8 mbar H_2 gas at RT, 500, 700, and 750 °C for 0.5 h. (e-h) EELS spectra and ED patterns acquired after exposure to 3.5 mbar CO_2 gas at 100 °C for 0.5 h after a preceding H_2 exposure for 1 h at 650 °C. The EELS fine structure of C-K, Ti-$L_{3,2}$, and O-K is presented. Note the x2 factor for O-K.

Experimental Section

$Ti_3C_2T_x$ MXene multilayer powder used in the ETEM experiments was prepared by chemical etching of Ti_3AlC_2 powder that in turn was synthesized following a procedure previously described. [31] One gram of $Ti_3C_2T_x$ powder was immersed and continuously stirred in 20 ml aqueous solution of LiF and HCl acid with 1.5:12 molar ratio for 24 h at 35 °C. After etching, the mixture was washed three times each by 40 ml of 1 M HCl to remove all the excess LiF salts followed by 3 cycles of washes with 40 ml of 1 M LiCl each. The mixture was then washed with deionized (DI) water for several cycles each of 40 ml until the supernatant reached a pH of approximately 6. Delamination into (20 μm x 20 μm) single flakes in deaerated DI-water was facilitated by gentle shaking for 10 minutes followed by centrifuging at 3500 rpm for 1 h. TEM samples were thereafter prepared by drop-casting 0.1 μl single-flake-solution on a DENSsolutions through hole Wildfire nanochip and placed in a DENSsolutions Wildfire single-tilt heating holder. The image corrected FEI Titan ETEM at DTU equipped with a high brightness XFEG and a monochromator operated at 300 kV achieving ~0.8 Å resolution was used to characterize the surfaces of single flakes. H_2, N_2, and CO_2 gas was introduced separately at temperatures ranging from room temperature up to 750 °C for pressures between $\sim 10^{-6}$ mbar $-$ 8 mbar and the samples were characterized before, during, and after exposure. EELS was acquired in diffraction mode resulting in ~0 mrad convergence angle and a ~10 mrad collection angle with a GIF Tridiem spectrometer at ~1.3 eV energy resolution and 0.2 eV energy dispersion. EELS spectra were acquired in high vacuum conditions after gas exposure on regions that had not been subjected to the electron beam. EELS data processing was performed using the commercial Gatan Digital Micrograph software with built in routines. Quantification was done on single scattering distributions after Fourier deconvolution, power-law background subtraction, and employing Hartree-Slater inelastic electron scattering cross-sections, excluding energy-loss near edge structures. RGA data was acquired with a Pfeiffer Vacuum mass spectrometer. HRTEM images were acquired with Gatan OneView 4K CMOS camera. First-principle calculations were performed using DFT, see details in the supplementary information.

Acknowledgements

The authors acknowledge the Swedish Research Council for funding under grants no. 2016-04412, 2016-00889 and 642-2013-8020. The Knut and Alice Wallenberg's Foundation is acknowledged for support of the electron microscopy laboratory in Linköping, a Fellowship grant and a project grant (KAW 2015.0043). The authors also acknowledge Swedish Foundation for Strategic Research (SSF) through project funding (EM16-0004) and the Research Infrastructure Fellow program no. RIF 14-0074 and no. FL12-0181. The authors finally acknowledge support from the Swedish Government Strategic Research Area in Materials Science on Functional Materials at Linköping University (Faculty Grant SFO-Mat-LiU No 2009 00971).

Author contributions

P.O.Å. P. conceived the research plan with input from L.-Å. N., I. P., and J. R.

The materials were prepared by J. H.

I.P. performed the experimental work and the analysis under supervision of T.W.H., J.B.W., J.P., J.R., V.D and P.O.Å.P.

H. L. performed the first-principle calculations and analysis under supervision of J.R.

The manuscript was drafted by I.P. and P.O.Å.P and finalized with input from all authors.

Competing interests

The authors declare no competing interests

References

[1] S. Choi, J.H. Drese, C.W. Jones, *Chem. Sus. Chem.*, **2009**, 2, 796.

[2] J. Zhang, R. Singh, P.A. Webley, *Micropor. Mesopor. Mater.*, **2008**, 111, 478.

[3] C.A. Trickett, A. Helal, B.A. Al-Maythalony, Z.H. Yamani, K.E. Cordova, O.M. Yaghi, *Nat. Rev. Mater.*, **2017**, 2, 17045.

[4] X. Li, Y. Cheng, H. Zhang, S. Wang, Z. Jiang, R. Guo, and H. Wu, *ACS Appl. Mater. Interfaces*, **2015**, 7, 5528.

[5] R. Ben-Mansour, M.A. Habib, O.E. Bamidele, M. Basha, N.A.A. Qasem, A. Peedikakkal, T. Laoui, and M. Ali, *Appl. Energy*, **2016**, 161, 225.

[6] M. Naguib, V.N. Mochalin, M.W. Barsoum, Y. Gogotsi, *Adv. Mater.*, **2014**, 26, 992.

[7] M. Ghidiu, M.R. Lukatskaya, , M.-Q. Zhao , Y. Gogotsi, and M.W. Barsoum, *Nature,* **2014**, 516, 78.

[8] B. Anasori, M.R. Lukatskaya and Y. Gogotsi, *Nat. Rev. Mater.*, **2017**, 2, 16098.

[9] F. Shahzad, M. Alhabeb, C.B. Hatter, B. Anasori, S. Man Hong, C.M. Koo, Y. Gogotsi, *Science* **2016**, 353, 1137.

[10] Q. Peng, J. Guo, Q. Zhang, J. Xiang, B. Liu, A. Zhou, R. Liu, Y. Tian, *J. Am. Chem. Soc.* **2014**, 136, 4113.

[11] M. Naguib, M. Kurtoglu, V. Presser, J. Lu, J.J. Niu, M. Heon, L. Hultman, Y. Gogotsi and M.W. Barsoum, *Adv. Mater.*, **2011**, 23, 4248.

[12] M. Naguib, O. Mashtalir, J. Carle, V. Presser, J. Lu, L. Hultman, Y. Gogotsi and M.W. Barsoum, *ACS Nano*, **2012**, 6, 1322.

[13] M.W. Barsoum, *Prog. Solid State Chem.* **2000**, 28, 201.

[14] P. Srivastava, A. Mishra, H. Mizuseki, K.-R. Lee, and A.K. Singh, *ACS Appl. Mater. Interfaces*, **2016**, 8, 24256

[15] M. Naguib, J. Halim, J. Lu, L. Hultman, Y. Gogotsi, and M.W. Barsoum, *J. Amer. Chem. Soc.,* **2013***,* 135, 15966.

[16] B. Anasori, Y. Xie, M. Beidaghi, J. Lu, B.C. Hosler, L. Hultman, P.R.C. Kent, Y. Gogotsi and M.W. Barsoum, *ACS Nano*, **2015**, 9, 9507.

[17] I. Persson, A. el Ghazaly, Q. Tao, J. Halim, S. Kota, V. Darakchieva, J. Palisaitis, M.W. Barsoum, J. Rosen, and P.O.Å. Persson *Small*, **2018**, 14, 1703676.

[18] Q. Tao, M. Dahlqvist, J. Lu, S. Kota, R. Meshkian, J. Halim, J. Palisaitis, L. Hultman, M. W. Barsoum, P. O.Å. Persson and J. Rosen, *Nat. Commun.*, **2017**, 8, 14949.

[19] R. Meshkian, M. Dahlqvist, J. Lu, B. Wickman, J. Halim, J. Thörnberg, Q. Tao, S. Li, S. Intikhab, J. Snyder, M.W. Barsoum, M. Yildizhan, J. Palisaitis, L. Hultman, P.O.Å. Persson, and J. Rosen, *Adv. Mater*., **2018**, 30, 1706409.

[20] M. Khazaei, A. Ranjbar, M. Arai, T. Sasaki and S. Yunoki *J. Mater. Chem. C,* **2017**, 5, 2488.

[21] Á. Morales-García, A. Fernández-Fernández, F. Viñes, and F. Illas, *J. Mater. Chem. A,* **2018**, 6, 3381.

[22] N. Li, X. Chen, W.-J. Ong, D.R. MacFarlane, X. Zhao, A. K. Cheetham, and C. Sun, *ACS Nano*, **2017**, 11, 10825.

[23] Y. Shao, F. Zhang, X. Shi, and H. Pan, *Phys. Chem. Chem. Phys.*, **2017**, 19, 28710.

[24] M.A. Hope, A.C. Forse, K.J. Griffith, M.R. Lukatskaya, M. Ghidiu, Y. Gogotsi, and C.P. Grey, *Phys. Chem. Chem. Phys.*, **2016**, 18, 5099.

[25] I. Persson, L.-Å. Näslund, J. Halim, M.W. Barsoum, J. Palisaitis, V. Darakchieva, J. Rosen, and P.O.Å. Persson, *2D Materials,* **2017**, 5, 015002.

[26] M. Khazaei, M. Arai, T. Sasaki, C.-Y. Chung, N.S. Venkataramanan, M. Estili, Y. Sakka, and Y. Kawazoe, *Adv. Funct. Mater.*, **2013**, 23, 2185.

[27] L.H. Karlsson, J. Birch, J. Halim, M.W. Barsoum, and P.O.Å. Persson, *Nano Lett.*, **2015**, *15*, 4955.

[28] X. Sang, Y. Xie, D.E. Yilmaz, R. Lotfi, M. Alhabeb, A. Ostadhossein, B. Anasori, W. Sun, X. Li, K. Xiao, P.R.C. Kent, A.C.T. van Duin, Y. Gogotsi and R.R. Unocic, *Nature Commun.*, **2018**, 9, 2266.

[29] Z. R. Herm, J. A. Swisher, B. Smit, R. Krishna, and J. R. Long, *J. Am. Chem. Soc.*, **2011**, 133, 5664.

[30] S. Cavenati, C. A. Grande, and A. E. Rodrigues, *J. Chem. Eng. Data,* **2004**, 49, 1095.

[31] A. Miranda, J. Halim, M.W. Barsoum, A. Lorke. *Appl. Phys. Lett*., **2016**, 108, 033102.